Electrical Power and Energy Systems 130 (2021) 106958

Contents lists available at ScienceDirect

International Journal of Electrical Power and Energy Systems

journal homepage: www.elsevier.com/locate/ijepes

Phasor-based fault location algorithm for three-end multi-section nonhomogeneous parallel transmission lines

Ahmed Saber [a,*], Bhavesh R. Bhalja [b]

[a] Electrical Power Engineering Department, Cairo University, Giza, Egypt
[b] Department of Electrical Engineering, Indian Institute of Technology, Roorkee, India

ARTICLE INFO

Keywords:
Current phasors
Fault location
Transmission lines

ABSTRACT

In order to estimate the fault location on three-terminal multi-section mixed nonhomogeneous transmission lines, all the previously published algorithms utilize the synchronized voltage and current measurements at all ends. In this article, a fault location algorithm for three-terminal multi-section mixed double-circuit untransposed transmission lines is presented utilizing only unsynchronized current measurements. Considering issues related to the shunt capacitance, un-transposition of the line, and mutual couplings between all phases, a threshold free identification algorithm is developed to differentiate the faulted line branch. In addition, analytical fault location equation is deduced independent of fault resistance and fault type. The three-terminal power system is modeled using MATLAB environment, and several fault cases are conducted, including all fault types, different fault resistances and locations, as well as different fault inception angles. The introduced work shows high accuracy under the effect of measurement and synchronization errors as well as line parameters errors.

1. Introduction

Tapped and multi-terminal transmission lines are reasonably economical solution to overcome right of way limitations. These lines can be constructed without installing a substation at the tee-node [1]. As there are absorbed or injected currents at the tee-node, identification of fault point for tapped and multi-terminal transmission lines is more complicated than that for two-end transmission lines. Several algorithms have been presented to resolve the issue of fault location for tapped [2,3] and multi-terminal [3–17] single-circuit homogeneous transmission lines. In addition, few algorithms have discussed the issue of fault location for multi-terminal double-circuit homogeneous transmission lines [18–23]. Due to cross-circuit faults and influence of potential couplings between parallel circuits, identification of fault point for tapped double-circuit transmission lines is more complicated than that of tapped single-circuit transmission lines. In [18], wavelet transform and travelling waves are integrated to determine the fault location on tapped parallel transmission lines employing the three ends measurements. In this algorithm, the fault resistance above 100 Ω and the mutual couplings between lines have a significant impact on the precision of the algorithm and it is not effective for cross-circuit faults. In [19], a fault location algorithm has been introduced for three-end parallel transmission lines. Though the said algorithm is not affected by fault type or fault resistance, the three ends synchronized voltage and current measurements are required. Also, its performance is highly affected by errors in line parameters. Afterwards, to obtain the faulted branch and the fault location, an algorithm based on three-end synchronized sequence components of voltages and currents is presented for three-end double-circuit transmission lines [20]. However, the mutual coupling between the two circuits is not considered in fault location calculations. In addition, the above method is not applicable for ungrounded faults. In [21], a fault location scheme based on negative-sequence network has been presented for three-end parallel transmission line utilizing one-terminal measurements. In addition, the mutual coupling between the two circuits has a limited effect on fault location accuracy. However, the said scheme is not applicable for cross-circuit faults. Thereafter, two fault location schemes are formulated, which utilize lumped parameters of transmission lines [22,23]. Nevertheless, the aforementioned methods are not applicable for long transmission line due to non-consideration of the line shunt capacitance.

To summarize, the algorithms mentioned in [2–23] are not applicable for estimation of fault location on multi-section nonhomogeneous transmission lines. Subsequently, several other algorithms have discussed the issue of fault location for two-end multi-section mixed

* Corresponding author.
E-mail address: a_saber_86@yahoo.com (A. Saber).

https://doi.org/10.1016/j.ijepes.2021.106958
Received 22 October 2020; Received in revised form 29 December 2020; Accepted 24 February 2021
Available online 29 March 2021

transmission lines [24–33]. These algorithms are based on soft computing technique [24], travelling waves [25–28], and impedance [29–33]. The soft computing based algorithms cannot be applied to new transmission lines configurations as manual training data are needed initially. Travelling waves algorithms require high sampling rate and the detection of wave head is highly affected by the fault resistance and errors in line parameters. Due to variation in the value of propagation velocity because of different frequencies of travelling waves, it is difficult to determine the propagation velocity at a certain frequency. Conversely, impedance based algorithms have discussed the issue of fault location for three-end multi-section mixed transmission lines [34,35] and multi-end mixed transmission lines [36–38]. In [34], synchronized positive-sequence components data are utilized to obtain the faulted branch and fault location on three-end hybrid parallel transmission lines. Though the said method is independent of fault resistance, fault type, and source impedance, line un-transposition and the potential couplings among the circuits are ignored as both circuits are treated as two separate circuits. Thereafter, a fault location impedance-based algorithm has been presented for three-end hybrid parallel transmission lines [35]. However, this algorithm requires synchronized three-end voltage and current measurements. In [36–38], positive-sequence components are utilized to determine the faulted branch and fault location on multi-end hybrid transmission lines. However, the aforementioned algorithms require the multi-end synchronized voltage and current data.

In order to rectify the said problems, a new fault location algorithm is introduced in this article for three-end mixed double-circuit multi-section transmission lines. Three main contributions of the proposed approach are as under.

- Unlike other previous algorithms [34–38], the suggested scheme does not require time synchronization. Therefore, the problems associated with time synchronization errors are avoided.
- The introduced work utilizes only the current measurements at the three ends unlike previous algorithms [34–38] that use both voltage and current measurements.
- The proposed algorithm provides higher fault distance estimation accuracy considering errors in line parameters compare to previously published algorithms [34–38].

The work is organized as follows. The introduced algorithm is discussed in Section 2. The simulation studies are presented in Sections 3 and 4 summarizes the proposed work.

2. Proposed fault location algorithm

2.1. Studied power system

The studied system is presented in Fig. 1 for three-end multi-section mixed parallel untransposed transmission lines composing of three line branches (*S-Q*), (*R-Q*), and (*T-Q*). The line branches (*S-Q*), (*R-Q*), and (*T-Q*) compose of three, two, and two line sections with line lengths (L_S, L_{S1}, and L_{S2}), (L_R and L_{R1}), and (L_T and L_{T1}), respectively. In addition, three loads are installed at *S*, *R*, and *T* buses.

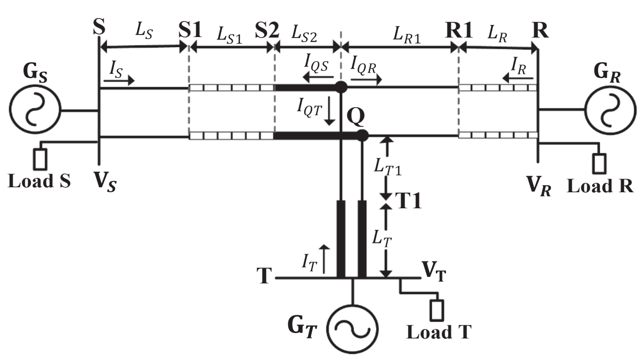

Fig. 1. Studied power system.

The proposed fault location algorithm consists of two steps. The 1st step is to recognize the faulted line branch as explained in the following Section 2.2. The 2nd step is to determine the faulted section and fault location as explained in the following Section 2.3.

2.2. Faulted branch recognition

Firstly, the faulted branch is distinguished to minimize the three-end network to two-end network. The PI line model is used to represent the line shunt capacitance. The voltage and current phasors at the end of line section (*S-S1*) are given by (1) [39].

$$\begin{bmatrix} V_{S1} \\ I_{S1} \end{bmatrix} = \begin{bmatrix} 1+0.5\times A_S & Z_S L_S \\ B_S & 1+0.5\times A_S \end{bmatrix} \begin{bmatrix} V_S \\ -I_S \end{bmatrix} \tag{1}$$

where V_S, V_{S1}, I_S, and I_{S1} are, respectively, 6×1 voltage and current phasors at *S* and *S1* ends. Z_S and Y_S are, respectively, 6×6 impedance and admittance of section (*S-S1*) per-unit length. The matrices A_S and B_S are given by (2).

$$A_S = (L_S)^2 Y_S Z_S \& B_S = Y_S L_S (1+0.25\times A_S) \tag{2}$$

As the elements of V_S in both circuits are equal for similar phases, the voltage difference between similar phases in both circuits is given by (3).

$$\Delta V_S = \begin{bmatrix} V_{S,a1}-V_{S,a2} \\ V_{S,b1}-V_{S,b2} \\ V_{S,c1}-V_{S,c2} \end{bmatrix} = \begin{bmatrix} 0 \\ 0 \\ 0 \end{bmatrix} \tag{3}$$

where *a*, *b*, and *c* represent the phases of circuit-1 or circuit-2. Accordingly, (1) is rewritten as:

$$\begin{bmatrix} \Delta V_{S1} \\ \Delta I_{S1} \end{bmatrix} = -\begin{bmatrix} \Delta Z_S L_S \\ 1+0.5\times \Delta A_S \end{bmatrix} \Delta I_S \tag{4}$$

where

$$\Delta I_S = \begin{bmatrix} I_{S,a1}-I_{S,a2} \\ I_{S,b1}-I_{S,b2} \\ I_{S,c1}-I_{S,c2} \end{bmatrix} \& \Delta I_{S1} = \begin{bmatrix} I_{S1,a1}-I_{S1,a2} \\ I_{S1,b1}-I_{S1,b2} \\ I_{S1,c2}-I_{S1,c2} \end{bmatrix} \tag{5}$$

ΔZ_S and ΔA_S are, respectively, shown in (6) and (7).

$$\Delta Z_S = \begin{bmatrix} Z_S(a_1,a_1)-Z_S(a_2,a_1) & Z_S(a_1,b_1)-Z_S(a_2,b_1) & Z_S(a_1,c_1)-Z_S(a_2,c_1) \\ Z_S(b_1,a_1)-Z_S(b_2,a_1) & Z_S(b_1,b_1)-Z_S(b_2,b_1) & Z_S(b_1,c_1)-Z_S(b_2,c_1) \\ Z_S(c_1,a_1)-Z_S(c_2,a_1) & Z_S(c_1,b_1)-Z_S(c_2,b_1) & Z_S(c_1,c_1)-Z_S(c_2,c_1) \end{bmatrix} \tag{6}$$

$$\Delta A_S = \begin{bmatrix} A_S(a_1,a_1)-A_S(a_2,a_1) & A_S(a_1,b_1)-A_S(a_2,b_1) & A_S(a_1,c_1)-A_S(a_2,c_1) \\ A_S(b_1,a_1)-A_S(b_2,a_1) & A_S(b_1,b_1)-A_S(b_2,b_1) & A_S(b_1,c_1)-A_S(b_2,c_1) \\ A_S(c_1,a_1)-A_S(c_2,a_1) & A_S(c_1,b_1)-A_S(c_2,b_1) & A_S(c_1,c_1)-A_S(c_2,c_1) \end{bmatrix} \tag{7}$$

Similarly, the voltage and current phasors at the end of line section (*S1-S2*) are given by (8).

$$\begin{bmatrix} \Delta V_{S2} \\ \Delta I_{S2} \end{bmatrix} = \begin{bmatrix} 1+0.5\times \Delta A_{S1} & \Delta Z_{S1} L_{S1} \\ \Delta B_{S1} & 1+0.5\times \Delta A_{S1} \end{bmatrix} \begin{bmatrix} \Delta V_{S1} \\ \Delta I_{S1} \end{bmatrix} \tag{8}$$

where ΔZ_{S1}, ΔA_{S1}, and ΔB_{S1} are written similar to ΔZ_S and ΔA_S in (6) and (7). Similarly, the voltage and current phasors at the end of line section (*S2-Q*) are given by (9).

$$\begin{bmatrix} \Delta V_{QS} \\ \Delta I_{QS} \end{bmatrix} = \begin{bmatrix} 1+0.5\times \Delta A_{S2} & \Delta Z_{S2} L_{S2} \\ \Delta B_{S2} & 1+0.5\times \Delta A_{S2} \end{bmatrix} \begin{bmatrix} \Delta V_{S2} \\ \Delta I_{S2} \end{bmatrix} \tag{9}$$

Following the same procedure for line branch (R-Q), the equations are given by (10)–(13).

$$\begin{bmatrix} \Delta V_{R1} \\ \Delta I_{R1} \end{bmatrix} = -\begin{bmatrix} \Delta Z_R L_R \\ 1 + 0.5 \times \Delta A_R \end{bmatrix} \Delta I_R e^{j\delta_{RS}} \tag{10}$$

$$\begin{bmatrix} \Delta V_{QR} \\ \Delta I_{QR} \end{bmatrix} = \begin{bmatrix} 1 + 0.5 \times \Delta A_{R1} & \Delta Z_{R1} L_{R1} \\ \Delta B_{R1} & 1 + 0.5 \times \Delta A_{R1} \end{bmatrix} \begin{bmatrix} \Delta V_{R1} \\ \Delta I_{R1} \end{bmatrix} e^{j\delta_{RS}} \tag{11}$$

where δ_{RS} is the phase difference angle between both ends R and S as end S is selected as a time reference. I_R is the current phasor at end R. V_{R1}, V_{QR}, I_{R1}, and I_{QR} are, respectively, 6×1 voltage and current phasors at end *R1* and tapping-node *Q*. Z_R, Z_{R1}, Y_R, and Y_{R1} are, respectively, 6×6 impedances and admittances of sections (*R-R1*) and (*R1-Q*) in per-unit length. A_R, A_{R1}, B_R, and B_{R1} are equal:

$$A_R = (L_R)^2 Y_R Z_R \& B_R = Y_R L_R (1 + 0.25 \times A_R) \tag{12}$$

$$A_{R1} = (L_{R1})^2 Y_{R1} Z_{R1} \& B_{R1} = Y_{R1} L_{R1} (1 + 0.25 \times A_{R1}) \tag{13}$$

Likewise, for line branch (*T-Q*), the equations are given by (14) and (15).

$$\begin{bmatrix} \Delta V_{T1} \\ \Delta I_{T1} \end{bmatrix} = -\begin{bmatrix} \Delta Z_T L_T \\ 1 + 0.5 \times \Delta A_T \end{bmatrix} \Delta I_T e^{j\delta_{TS}} \tag{14}$$

$$\begin{bmatrix} \Delta V_{QT} \\ \Delta I_{QT} \end{bmatrix} = \begin{bmatrix} 1 + 0.5 \times \Delta A_{T1} & \Delta Z_{T1} L_{T1} \\ \Delta B_{T1} & 1 + 0.5 \times \Delta A_{T1} \end{bmatrix} \begin{bmatrix} \Delta V_{T1} \\ \Delta I_{T1} \end{bmatrix} e^{j\delta_{TS}} \tag{15}$$

where δ_{TS} is the phase angle difference between T and S ends. I_T is the current phasor at end T. V_{T1}, V_{QT}, I_{T1}, and I_{QT} are, respectively, 6×1 voltage and current phasors at end *T1* and tapping-node *Q*. Z_T, Z_{T1}, Y_T, and Y_{T1} are, respectively, 6×6 impedances and admittances of sections (*T-T1*) and (*T1-Q*) in per-unit length. A_T, A_{T1}, B_T, and B_{T1} are given by (16) and (17).

$$A_T = (L_T)^2 Y_T Z_T \& B_T = Y_T L_T (1 + 0.25 \times A_T) \tag{16}$$

$$A_{T1} = (L_{T1})^2 Y_{T1} Z_{T1} \& B_{T1} = Y_{T1} L_{T1} (1 + 0.25 \times A_{T1}) \tag{17}$$

It is clear that the differential components (ΔV_{QS}, ΔV_{QR}, ΔV_{QT}, ΔI_{QS}, ΔI_{QR}, and ΔI_{QT}) can only be calculated utilizing the currents phasors (I_S, I_R, and I_T). The three values (ΔV_{QS}, ΔV_{QR}, and ΔV_{QT}) are approximately equal in normal conditions based on Kirchhoff voltage law (KVL). In addition, two of them are approximately equal in case of line faults and those are corresponding to the non-faulty branches. Now, assume that:

$$\Delta V_{SR} = maximum\{|\{|\Delta V_{QS}| - |\Delta V_{QR}|\}|\} \tag{18}$$

$$\Delta V_{RT} = maximum\{|\{|\Delta V_{QR}| - |\Delta V_{QT}|\}|\} \tag{19}$$

$$\Delta V_{ST} = maximum\{|\{|\Delta V_{QS}| - |\Delta V_{QT}|\}|\} \tag{20}$$

where "| |" represents the absolute value. Here, only the absolute values of ΔV_{QS}, ΔV_{QR}, and ΔV_{QT} are utilized as both phase difference angles (δ_{RS} and δ_{TS}) are unknown. Mathematically, the minimum value of ΔV_{SR}, ΔV_{RT}, and ΔV_{ST} is equal to the differential component of both healthy line branches. For example, if the minimum value is ΔV_{RT}, this denotes that both ΔV_{QR} and ΔV_{QT} are approximately equal. Accordingly, both branches (*R-Q*) and (*T-Q*) are healthy and the line branch (*S-Q*) is faulted. As a result, the faulted branch is recognized employing (18), (19), and (20) and only the unsynchronized current phasors are used.

2.3. Proposed fault location

After distinguishing the faulted branch, the final step is to differentiate the faulted section and find the fault point. In Fig. 2, assume that a fault occurs in section (*R1-Q*) at a distance of D_{FR1} per-unit from node *R1*. As both branches (*S-Q*) and (*T-Q*) are not faulted, both values ΔV_{QS} and ΔV_{QT} can be computed from (9) and (15), respectively. In order to calculate the phase difference angle (δ_{TS}), ΔV_{QS} and ΔV_{QT} are equal based on KVL and given by (21).

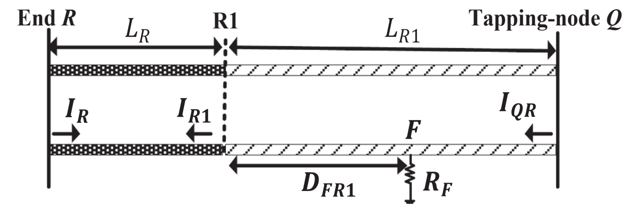

Fig. 2. Fault in line section (*R1-Q*).

$$Arg(\Delta V_{QS}) = Arg(\Delta V_{QT}) \tag{21}$$

where $Arg(\bullet)$ represents the phase angle. Accordingly, both ends S and T can be synchronized with each other solving (21) and the value (ΔI_{QR}) can also be calculated from (22).

$$\Delta I_{QR} = -(\Delta I_{QS} + \Delta I_{QT}) \tag{22}$$

At this stage, the fault location problem is minimized to two-end multi-section mixed lines and the unsynchronized differential components at both ends ($\Delta V_S = 0$, ΔV_{QR}, ΔI_S, and ΔI_{QR}) are known. To differentiate the faulted section and find the fault distance, suppose that each section is the faulted section and the corresponding fault distance is calculated [34–38]. For example, to find the fault distance for section (*R1-Q*), the differential components (ΔV_{R1} and ΔI_{R1}) are calculated from (10). ΔV_{FR1} at point F is given by (23).

$$[\Delta V_{FR1}] = \begin{bmatrix} 1 + 0.5 \times \Delta A_{FR1} & \Delta Z_{FR1} \end{bmatrix} \begin{bmatrix} \Delta V_{R1} \\ \Delta I_{R1} \end{bmatrix} e^{j\delta_{RS}} \tag{23}$$

$$A_{FR1} = (D_{FR1} \times L_{R1})^2 Y_{R1} Z_{R1} \tag{24}$$

$$Z_{FR1} = D_{FR1} \times L_{R1} \times Z_{R1} \tag{25}$$

The differential component (ΔV_{FQ}) at point F is given by (26).

$$[\Delta V_{FQ}] = \begin{bmatrix} 1 + 0.5 \times \Delta A_{FQ} & \Delta Z_{FQ} \end{bmatrix} \begin{bmatrix} \Delta V_{QR} \\ -\Delta I_{QR} \end{bmatrix} \tag{26}$$

$$A_{FQ} = ((1 - D_{FR1}) \times L_{R1})^2 Y_{R1} Z_{R1} \tag{27}$$

$$Z_{FQ} = (1 - D_{FR1}) \times L_{R1} \times Z_{R1} \tag{28}$$

Based on KVL, both values (ΔV_{FR1} and ΔV_{FQ}) are equal:

$$|\Delta V_{FR1}| = |\Delta V_{FQ}| \tag{29}$$

Only the absolute values of (ΔV_{FR1} and ΔV_{FQ}) are utilized as the phase difference angle (δ_{RS}) is unknown. As a result, the only unknown variable in (29) is D_{FR1} and this equation is accordingly solved to determine the value of D_{FR1}. Similarly, the fault distance (D_{FR}) can be obtained for section (*R-R1*). As expected, if the section (*R-R1*) is faulted, the value of D_{FR} will be between 0 and 1 per-unit and the other value of D_{FR1} will be negative. On the other hand, if the section (*R1-Q*) is faulted, the value of D_{FR} will exceed 1 per-unit and the other value of D_{FR1} will be between 0 and 1 per-unit. Similarly, the faulted section and the fault location can be obtained, if the fault occurs in branch (*S-Q*) or branch (*T-Q*). The detailed flowchart of the proposed algorithm is presented in Fig. 3.

3. Results and discussions

With reference to Fig. 1, Loads of 100 MVA are installed at *S*, *R*, and *T* buses and all lines lengths along with lines parameters data are shown in Appendix A, whereas all generators data are obtained from [35]. The current signals are passed through a low-pass 2nd order Butterworth filter with a cut-off frequency of 400 Hz. In addition, the data are sampled at a sampling frequency of 2.5 kHz and a digital mimic filter is employed to minimize the dc components. Consequently, one-cycle

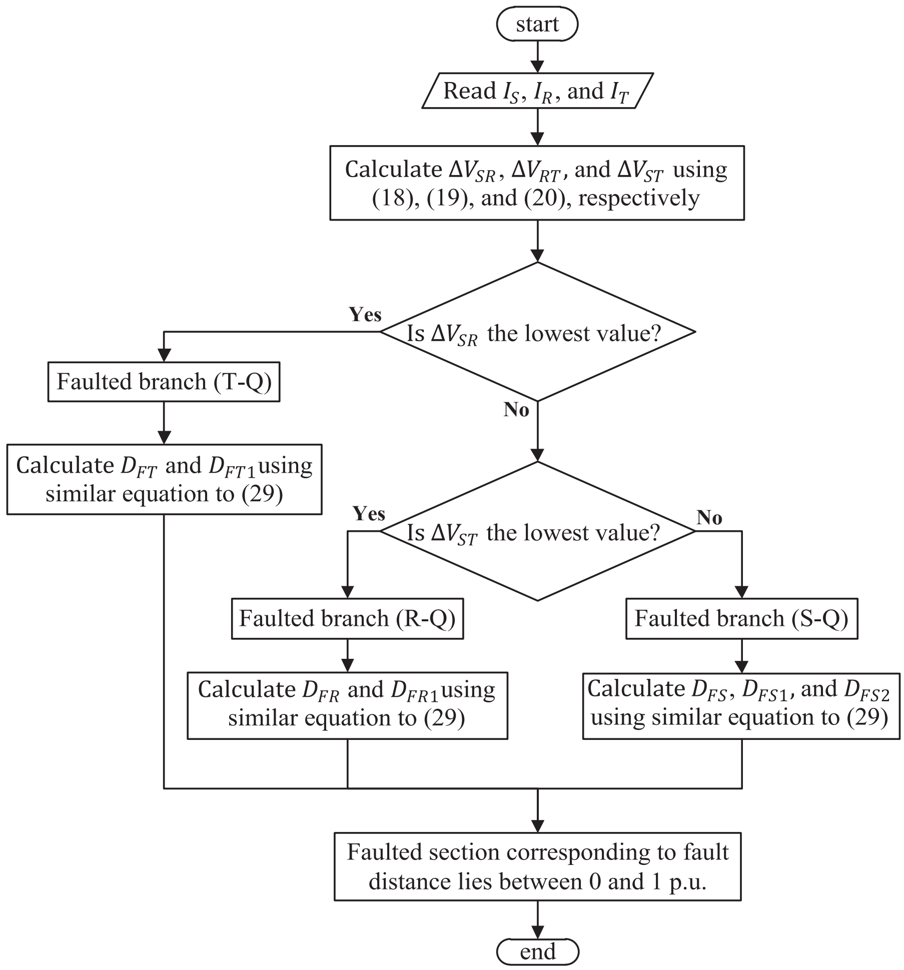

Fig. 3. The steps of the proposed algorithm.

discrete Fourier transform algorithm is used to estimate the three-end 50 Hz current phasors (I_S, I_R, and I_T) in the phase-domain.

Several fault cases are conducted on MATLAB program. Each line branch and each section is investigated by varying the fault resistance (R_F), fault location (D_F), and fault inception angle (δ_F). In addition, normal-shunt faults and cross-circuit faults are considered. Further, the system is examined under the influence of measurement and synchronization errors, as well line parameters estimation errors. The fault location error is calculated as per (30).

$$Error\ (\%) = \frac{|Calculated\ \ D_F(p.u.) - Actual\ \ D_F(p.u.)| \times Line\ \ Section\ \ length}{Total\ \ length\ \ of\ \ line\ \ branch} \tag{30}$$

3.1. Normal-shunt faults and cross-circuit faults in different phases

The introduced algorithm is tested for normal-shunt and cross-circuit faults in different phases, and the results are depicted in Table 1. Three fault cases are conducted for each section, and the phase difference angles (δ_{SR}, δ_{RT}, and δ_{ST}) between the three ends are, respectively, considered at 60°, 60°, and 120°. In addition, the calculated synchronization angles are also depicted in Table 1. To distinguish the faulted branch and the fault distance for each line section, the values of (ΔV_{SR}, ΔV_{RT}, and ΔV_{ST}) are calculated and illustrated in Table 1. Also, the fault location errors are indicated in Table 1. For instance, in the 3rd case, inter-circuit fault is simulated on section (*S-S1*) in phases *b* and *c* of circuit-1 and phases *a* and *b* of circuit-2 at D_F of 0.9 per-unit, δ_F of 90°, and R_F of 0.01 Ω. To distinguish the faulted branch, the minimum value of three differential components (ΔV_{SR}, ΔV_{RT}, and ΔV_{ST}) are estimated. Accordingly, the two branches (*R-Q*) and (*T-Q*) are healthy and the branch (*S-Q*) is faulted. In addition, the phase difference angle (δ_{RT}) between both ends *R* and *T* is obtained and its value is 60.37°. Finally, the corresponding fault distance (D_F) for each line section between end *S* and tapping-node *Q* is estimated. The values of D_F are equal to 0.9048, −0.072, and −0.620 per-unit for sections (*S-S1*), (*S1-S2*), and (*S2-Q*), respectively. As the value of D_F for section (*S-S1*) is between 0 and 1 per-unit and the values of D_F for sections (*S1-S2*) and (*S2-Q*) are negative, the faulted line section is (*S-S1*) and the percentage error of fault location is 0.096%. As recorded in Table 1, the maximum percentage error is limited to 0.369%.

3.2. Inter-circuit faults in similar phases

The simulation results during inter-circuit faults with varying $R_F$and δ_F are shown in Table 2. As an example, case 7 is double-phase fault in both circuits "a_1b_1-a_2b_2" in section (*R-R1*) at D_F of 0.7 per-unit and δ_F of 135°. The values of R_F are set at 74 Ω and 75 Ω for circuit-1 and circuit-2, respectively. To distinguish the faulted branch, the three values (ΔV_{SR}, ΔV_{RT}, and ΔV_{ST}) are estimated and the value of ΔV_{ST} is found to be minimum. Accordingly, the two branches (*S-Q*) and (*T-Q*) are considered as healthy whereas the branch (*R-Q*) is treated as faulted. In addition, δ_{ST} between both ends *S* and *T* is obtained and it is equal to 119.98°. Finally, the corresponding fault distance (D_F) for each section between end *R* and tapping-node *Q* is estimated. The values of D_F are equal to 0.697 and −0.091 per unit for sections (*R-R1*) and (*R1-Q*), respectively. As the value of D_F for section (*R-R1*) is between 0 and 1 per-unit and the value

Table 1
Results for different line sections considering $\delta_{SR} = 60^{\circ}, \delta_{RT} = 60^{\circ}$, *and* $\delta_{ST} = 60^{\circ}$.

Section	Fault condition				ΔV_{SR} (p.u.)	ΔV_{RT} (p.u.)	ΔV_{ST} (p.u.)	Calculated synchro. angle			D_F (p.u.)			Faulted section	Abs. error (km)	F.L. error %
	Type	D_F (p.u.)	$\delta_F{}^{o}$	R_F (Ω)				δ°_{SR}	δ°_{RT}	δ°_{ST}	1st	2nd	3rd			
S-S1	b_1g	0.4	180	5	2.6390	**0.0011**	2.6402	——	60.54	——	**0.4003**	−0.434	−0.880	*S-S1*	0.015	0.006
	a_2c_2	0.1	0	90	1.4201	**0.0001**	1.4202	——	60.26	——	**0.1008**	−0.654	−0.971	*S-S1*	0.04	0.016
	b_1c_1g-a_2b_2g	0.9	90	0.01	2.8944	**0.0017**	2.8958	——	60.37	——	**0.9048**	−0.072	−0.620	*S-S1*	0.24	0.096
S1-S2	a_1b_1g	0.25	45	15	1.6343	**0.0012**	1.6355	——	59.93	——	1.3513	**0.2488**	−0.451	*S1-S2*	0.096	0.038
	$a_2b_2c_2$	0.8	180	0.1	1.3527	**0.0027**	1.3553	——	60.02	——	2.1378	**0.8074**	−0.115	*S1-S2*	0.592	0.237
	b_1g-c_2g	0.5	135	100	0.5953	**0.0008**	0.5962	——	60.43	——	1.6578	**0.5050**	−0.294	*S1-S2*	0.40	0.160
S2-Q	a_2b_2g	0.05	0	200	0.2019	**0.0005**	0.2024	——	60.02	——	2.5032	1.0822	**0.0494**	*S2-Q*	0.072	0.029
	b_1c_1	0.6	45	20	0.3661	**0.0028**	0.3686	——	59.95	——	3.8674	2.0097	**0.6064**	*S2-Q*	0.768	0.307
	a_1b_1-a_2c_2	0.85	90	0.5	0.1732	**0.0043**	0.1775	——	60.07	——	4.4115	2.4258	**0.8512**	*S2-Q*	0.144	0.058
	$a_2b_2c_2$	0.03	135	5	1.0974	**0.0022**	1.0996	——	60.012	——	2.489	1.0564	**0.0336**	*S2-Q*	0.432	0.173
R-R1	c_2g	0.1	135	55	0.8513	0.8514	**0.0002**	——	——	119.31	**0.0963**	−0.263	——	*R-R1*	0.148	0.093
	a_2b_2	0.7	90	150	0.4552	0.4555	**0.0003**	——	——	119.92	**0.6977**	−0.090	——	*R-R1*	0.092	0.057
	a_1c_1g-b_2c_2g	0.45	0	1	2.9712	2.9715	**0.0002**	——	——	119.55	**0.4464**	−0.160	——	*R-R1*	0.144	0.090
R1-Q	a_2c_2g	0.15	45	40	0.7234	0.7239	**0.0019**	——	——	119.92	1.5161	**0.1511**	——	*R1-Q*	0.132	0.083
	$a_1b_1c_1$	0.6	180	10	0.4907	0.4976	**0.0069**	——	——	120.00	3.0155	**0.6007**	——	*R1-Q*	0.084	0.053
	c_1g-a_2g	0.8	135	125	0.0714	0.0715	**0.0016**	——	——	120.00	3.7706	**0.8022**	——	*R1-Q*	0.264	0.165
	a_2b_2	0.03	180	0.1	1.5000	1.4985	**0.0015**	——	——	119.91	1.0912	**0.0274**	——	*R1-Q*	0.195	
T-T1	a_2c_2	0.95	0	3	**0.0022**	0.6024	0.6032	60.16	——	——	**0.9507**	−0.140	——	*T-T1*	0.14	0.050
	a_1b_1g	0.45	45	75	**0.0002**	0.7727	0.7726	59.34	——	——	**0.4506**	−1.511	——	*T-T1*	0.12	0.043
	a_1c_1-b_2c_2	0.2	180	0.6	**0.0015**	3.7856	3.7840	59.63	——	——	**0.1986**	−2.228	——	*T-T1*	0.28	0.100
	a_2g	0.03	90	20	**0.0002**	2.7398	2.7395	58.96	——	——	**0.0306**	−2.7466	——	*T-T1*	0.124	0.044
T1-Q	a_2g	0.5	90	140	**0.0006**	0.0813	0.0820	59.99	——	——	1.1691	**0.4871**	——	*T1-Q*	**1.032**	**0.369**
	$a_1b_1c_1$	0.1	135	25	**0.0027**	0.4846	0.4841	59.93	——	——	1.034	**0.0942**	——	*T1-Q*	0.464	0.166
	b_1c_1-a_2b_2	0.9	0	10	**0.0046**	0.0769	0.0767	59.93	——	——	1.318	**0.8934**	——	*T1-Q*	0.528	0.189

of D_F for section (*R1-Q*) is negative, the faulted line section is (*R-R1*) and the percentage error of fault location is 0.075. As observed from Table 2, the maximum recorded error is restricted to 0.489%. As recorded in Tables 1 and 2, the introduced algorithm is capable to obtain the faulted section and the fault point for all cases successfully.

It is to be noted that the suggested algorithm does not succeed if the fault occurs in the same phases of both circuits with the same value of fault resistance in both circuits. This is due to exactly equal values of the current phasors (I_S, I_R, and I_T) of similar phases in both circuits because of which deduced equations become invalid (due to equal values of ΔI_S, ΔI_R, and ΔI_T). However, in real field, the probability of occurrence of inter-circuit fault in the same phases of both circuits with the same value of fault resistance is very rare.

3.3. Errors in line parameters estimation and comparative evaluation

Aging of transmission lines or errors introduced in line parameters estimation have a negative influence on the precision of fault location. The introduced algorithm is checked against errors of ±10% in line parameters (impedance and admittance matrices) of all line sections at the same time. Comparative evaluation in terms of fault location error is shown in Fig. 4, where the results of the proposed algorithm are compared with those in [34]. In Fig. 4, the fault location error against the fault distance for a 2-phase to ground fault "a_1b_1g" in circuit-1 of section (*S1-S2*) with R_F of 1 Ω is presented. It is observed from Fig. 4 that both algorithms are capable to distinguish the faulted branch and the faulted section. The maximum error given by the proposed scheme is 0.211% whereas the maximum error given by the algorithm depicted in [34] is 1.776%.

3.4. Impact of neglecting line capacitance and synchronization errors

Neglecting the line shunt capacitance (LSC) has adverse effect on the accuracy of fault location. To investigate the effect of neglecting the LSC, Fig. 5 illustrates the fault location error against the fault distance for inter-circuit fault "a_1c_1g-b_2c_2g" on section (*T-T1*) with $R_F = 10$ Ω. where the maximum error is equal to 0.211% without neglecting the LSC. On the other hand, the maximum error has increased to 6.824% with neglecting the LSC.

In addition, unlike the algorithms described in [34] and [35], which have utilized the three-end synchronized voltage and current measurements for estimation of fault location, the proposed algorithm used unsynchronized current measurements (without the need for time synchronization between all ends). For the algorithm described in [35], as per IEEE standard [40], the maximum time synchronization error does not exceed ±31 μs, which is equivalent to angle error of ±0.56° for 50 Hz system. As the algorithm in [35] has shown better fault location accuracy compared with that in [34], the faults in Table 2 are repeated for the algorithm described in [35] with angle error of ±0.56°. The results for the proposed algorithm and the scheme mentioned in [35] are shown in Table 3. It is to be noted from Table 3 that both algorithms are able to distinguish the faulted branch and the faulted section successfully. Moreover, the average and maximum errors given by the proposed algorithm is equal 0.138% and 0.489%, respectively, which is comparable to 0.374% and 0.988% as given by the algorithm mentioned in [35], correspondingly.

The proposed algorithm achieves better results because it takes advantage of the fact that the voltage phasors of similar phase in both circuits are equal to each other in case of the double-circuit line. In other words, the voltage measurements are utilized implicitly as the voltage difference between each similar phases in both circuits is used in deriving the fault location equation. However, since this voltage

Table 2
Results for inter-circuit faults in the same phases in both circuits.

Section	Fault condition				ΔV_{SR} (p.u.)	ΔV_{RT} (p.u.)	ΔV_{ST} (p.u.)	Calculated synch. angle			D_F (p.u.)			Faulty section	Abs. error (km)	F.L error%
	Type	D_F (p.u.)	δ_F^o	R_F (Ω)				δ^o_{SR}	δ^o_{RT}	δ^o_{ST}	1st	2nd	3rd			
S-S1	c_1g-c_2g	0.2	135	90–91	0.0083	**0.0000**	0.0083	—	62.62	—	**0.2054**	−0.607	−0.933	*S-S1*	0.27	0.108
	b_1c_1-b_2c_2	0.8	90	1–2	0.0677	**0.0000**	0.0677	—	60.09	—	**0.8106**	−0.133	−0.677	*S-S1*	0.53	0.212
S1-S2	a_1b_1g-a_2b_2g	0.25	45	14–15	0.0524	**0.0000**	0.0525	—	59.98	—	1.3558	**0.2505**	−0.185	*S1-S2*	0.04	0.016
	$a_1b_1c_1$-$a_2b_2c_2$	0.9	0	0.1–0.2	0.0038	**0.0000**	0.0038	—	60.06	—	2.2907	**0.9114**	−0.053	*S1-S2*	0.912	0.365
S2-Q	a_1g-a_2g	0.6	180	200–201	0.0004	**0.0000**	0.0004	—	59.98	—	3.6492	2.0278	**0.5984**	*S2-Q*	0.192	0.077
	a_1c_1g-a_2c_2g	0.05	90	9–10	0.0244	**0.0001**	0.0245	—	59.96	—	2.4957	1.0904	**0.0531**	*S2-Q*	0.372	0.149
R-R1	a_1b_1-a_2b_2	0.7	135	74–75	0.0114	0.0115	**0.0000**	—	—	119.98	**0.6970**	−0.091	—	*R-R1*	0.12	0.075
	$a_1b_1c_1$-$a_2b_2c_2$	0.15	0	4–5	0.3688	0.3689	**0.0001**	—	—	119.95	**0.1503**	−0.253	—	*R-R1*	0.012	0.007
R1-Q	b_1g-b_2g	0.85	45	40–41	0.0013	0.0013	**0.0000**	—	—	120.01	3.7674	**0.8516**	—	*R1-Q*	0.192	0.120
	$a_1b_1c_1$-$a_2b_2c_2$	0.3	180	24–25	0.0204	0.0204	**0.0001**	—	—	119.99	2.0117	**0.3011**	—	*R1-Q*	0.132	0.082
T-T1	a_1c_1-a_2c_2	0.9	135	140–141	**0.0000**	0.0019	0.0020	59.98	—	—	**0.8996**	−0.285	—	*T-T1*	0.08	0.029
	b_1c_1g-b_2c_2g	0.1	90	0.5–0.6	**0.0000**	0.0390	0.0389	59.97	—	—	**0.1002**	−2.472	—	*T-T1*	0.04	0.014
T1-Q	$a_1b_1c_1$-$a_2b_2c_2$	0.5	0	15–16	**0.0001**	0.0085	0.0084	59.89	—	—	1.1754	**0.4934**	—	*T1-Q*	0.528	0.189
	a_1g-a_2g	0.1	45	59–60	**0.0000**	0.0026	0.0026	59.99	—	—	1.0288	**0.0829**	—	*T1-Q*	**1.368**	**0.489**

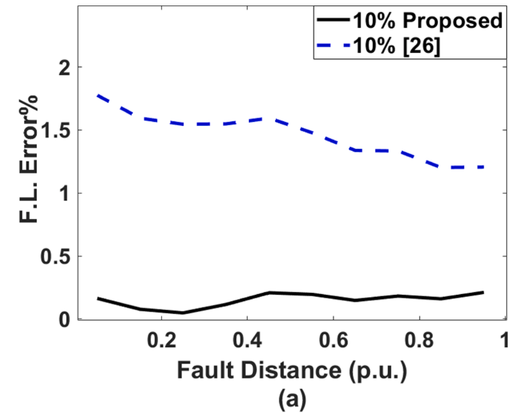

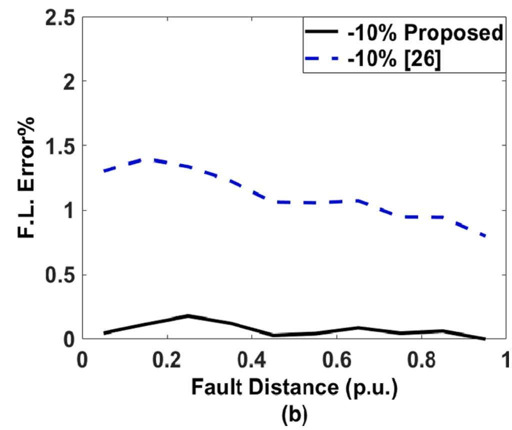

Fig. 4. Recorded percentage error under the impact of line parameters errors, (a) 10%, (b) −10%.

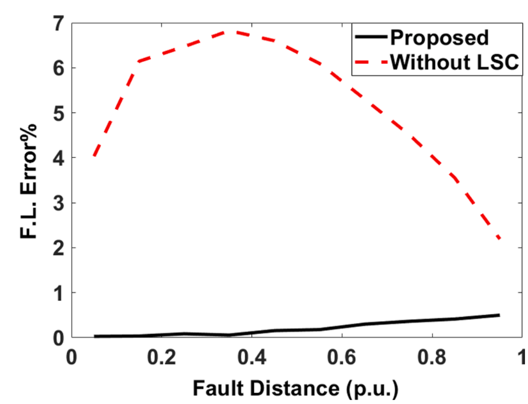

Fig. 5. Recorded percentage error under the impact of neglecting the line shunt capacitance.

difference is equal to zero in all cases because both circuits are connected to the same bus in case of the double-circuit line, there is no need to utilize the voltage measurements. In other words, there is no any possibility of error in voltage measurements or error in estimated voltage phasors. Furthermore, taking into consideration that the synchronization errors have a negative influence on the fault location accuracy of the algorithm described in [35], and the proposed algorithm does not require the current measurements to be synchronized as the phase difference angles are calculated. Therefore, the proposed work accomplishes better accuracy than the algorithm described in [35] with respect to synchronization errors.

Table 3
Comparative evaluation with considering synchronization errors.

Branch		Percentage error%					
		1st section		2nd section		3rd section	
		Proposed	[35]	Proposed	[35]	Proposed	[35]
S-Q	Average	0.108	0.154	0.016	0.237	0.077	0.485
	Maximum	0.212	0.406	0.365	0.080	0.149	0.206
R-Q	Average	0.075	**1.483**	0.120	0.218	——	——
	Maximum	0.007	0.095	0.082	0.623	——	——
T-Q	Average	0.029	0.450	0.189	0.240	——	——
	Maximum	0.014	0.086	**0.489**	0.357	——	——

3.5. *Impact of current transformer (CT) errors and small phase difference angles*

To consider smaller values of the phase difference angles and the effect of the CT errors, different fault cases are conducted considering CT magnitude error of $\pm5\%$ in current measurements, and the phase difference angles between the three ends (δ_{SR}, δ_{RT}, and δ_{ST}) are set at 2°, 3°, and 5°, respectively. The obtained results are depicted in Table 4, where these results are compared with that without considering the CT errors. It is observed from Table 4 that the maximum error in estimating the fault location considering the CT errors is equal to 1.92% whereas the same without considering the CT errors is equal to 0.372%. Though the fault location accuracy of the proposed algorithm is significantly affected by the CT measurement errors, it remains well below 5%.

Table 4
Results with considering CT errors.

Section	Fault condition				F.L. error%	
	Type	D_F (p.u.)	$\delta_F{}^o$	R_F (Ω)	Without CT Errors	With CT Errors
S-S1	a_1g	0.8	0	25	**0.372**	1.194
S1-S2	a_2b_2g	0.1	90	1	0.0531	1.337
S2-Q	a_1c_1	0.9	180	60	0.0715	1.495
R-R1	$a_2b_2c_2$	0.5	45	0.1	0.0428	0.257
R1-Q	b_2g	0.7	135	10	0.159	**1.920**
T-T1	a_1c_1g	0.2	180	90	0.0801	0.934
T1-Q	b_2c_c	0.85	0	5	0.243	1.348

4. Conclusions

This article has developed a novel fault location algorithm for three-end multi-section mixed double-circuit untransposed transmission lines. The proposed algorithm utilizes only unsynchronized current measurements at the three ends the lines. The effect of line shunt capacitance, un-transposition of the line, and mutual couplings between all phases is considered in derivation of fault location equation. In addition, the deduced analytical fault location equation is independent of fault type and resistance. Furthermore, a threshold free recognition algorithm is proposed to distinguish the faulted branch. The emulation studies emphasize that the proposed algorithm accomplishes high precision for several cases considering different fault resistance and fault locations as well as all fault types. In addition, the maximum recorded error of fault location does not exceed 0.489% considering the influence of $\pm10\%$ errors in line parameters. Furthermore, the proposed algorithm is not applicable when the fault occurs in similar phases of both circuits with the same value of fault resistance in both circuits. However, the probability of occurrence such faults is very rare in reality.

CRediT authorship contribution statement

Ahmed Saber: Conceptualization, Methodology, Investigation, Validation, Software, Writing - original draft. **Bhavesh R. Bhalja:** Conceptualization, Investigation, Writing - review & editing.

Declaration of Competing Interest

The authors declare that they have no known competing financial interests or personal relationships that could have appeared to influence the work reported in this paper.

Acknowledgement

This work was supported by Elsewedy Electric PSP Company.

Appendix A

The lengths of all line sections are:

Line Section	L_S	L_{S1}	L_{S2}	L_R	L_{R1}	L_T	L_{T1}
Length (km)	50	80	120	40	120	200	80

The impedance and admittance matrices for each line section are:

$$Z_{LS} = \begin{bmatrix} 0.0450+0.552i & 0.0226+0.227i & 0.0232+0.188i & 0.0218+0.155i & 0.0225+0.157i & 0.0232+0.153i \\ 0.0226+0.227i & 0.0465+0.564i & 0.0241+0.237i & 0.0225+0.157i & 0.0234+0.166i & 0.0241+0.167i \\ 0.0232+0.188i & 0.0241+0.237i & 0.0480+0.572i & 0.0232+0.153i & 0.0241+0.167i & 0.0248+0.175i \\ 0.0218+0.155i & 0.0225+0.157i & 0.0232+0.153i & 0.0450+0.552i & 0.0226+0.227i & 0.0232+0.188i \\ 0.0225+0.157i & 0.0234+0.166i & 0.0241+0.167i & 0.0226+0.227i & 0.0465+0.564i & 0.0241+0.237i \\ 0.0232+0.153i & 0.0241+0.167i & 0.0248+0.175i & 0.0232+0.188i & 0.0241+0.237i & 0.0480+0.572i \end{bmatrix} (\Omega/km)$$

$$Y_{LS1} = 10^{-5}\text{x}\begin{bmatrix} 0.2727i - 0.0609i - 0.0227i - 0.0204i - 0.0141i - 0.0086i \\ -0.0609i0.2885i - 0.0539i - 0.0141i - 0.0128i - 0.0098i \\ -0.0227i - 0.0539i0.2912i - 0.0086i - 0.0098i - 0.0099i \\ -0.0204i - 0.0141i - 0.0086i0.2727i - 0.0609i - 0.0227i \\ -0.0141i - 0.0128i - 0.0098i - 0.0609i0.2885i - 0.0539i \\ -0.0086i - 0.0098i - 0.0099i - 0.0227i - 0.0539i0.2912i \end{bmatrix}(S/km)$$

$$Z_{LS1} = Z_{LR} = Z_{LT1} = \begin{bmatrix} 0.0902 + 0.597i0.0620 + 0.298i0.0612 + 0.256i0.0635 + 0.271i0.0620 + 0.253i0.0612 + 0.241i \\ 0.0620 + 0.298i0.0875 + 0.598i0.0601 + 0.297i0.0620 + 0.253i0.0607 + 0.252i0.0600 + 0.253i \\ 0.0612 + 0.256i0.0601 + 0.297i0.0862 + 0.597i0.0612 + 0.241i0.0600 + 0.253i0.0595 + 0.271i \\ 0.0635 + 0.271i0.0620 + 0.253i0.0612 + 0.241i0.0902 + 0.597i0.0620 + 0.298i0.0612 + 0.256i \\ 0.0620 + 0.253i0.0607 + 0.252i0.0600 + 0.253i0.0620 + 0.298i0.0875 + 0.598i0.0601 + 0.297i \\ 0.0612 + 0.241i0.0600 + 0.253i0.0595 + 0.271i0.0612 + 0.256i0.0601 + 0.297i0.0862 + 0.598i \end{bmatrix}(\Omega/km)$$

$$Y_{LS1} = Y_{LR} = Y_{LT1} = 10^{-5}\text{x}\begin{bmatrix} 0.3079i - 0.0662i - 0.0221i - 0.0432i - 0.0224i - 0.0132i \\ -0.0662i0.3199i - 0.0584i - 0.0224i - 0.0187i - 0.0176i \\ -0.0221i - 0.0584i0.3247i - 0.0132i - 0.0176i - 0.0305i \\ -0.0432i - 0.0224i - 0.0132i0.3079i - 0.0662i - 0.0221i \\ -0.0224i - 0.0187i - 0.0176i - 0.0662i0.3199i - 0.0584i \\ -0.0132i - 0.0176i - 0.0305i - 0.0221i - 0.0584i0.3247i \end{bmatrix}(S/km)$$

$$Z_{LS2} = Z_{LR1} = Z_{LT} = \begin{bmatrix} 0.0830 + 0.635i0.0574 + 0.303i0.0570 + 0.259i0.0579 + 0.260i0.0574 + 0.253i0.0570 + 0.238i \\ 0.0574 + 0.303i0.0819 + 0.635i0.0566 + 0.302i0.0574 + 0.253i0.0569 + 0.260i0.0566 + 0.252i \\ 0.0570 + 0.260i0.0566 + 0.302i0.0814 + 0.635i0.0570 + 0.238i0.0566 + 0.252i0.0563 + 0.259i \\ 0.0579 + 0.260i0.0574 + 0.253i0.0570 + 0.238i0.0830 + 0.635i0.0574 + 0.303i0.0570 + 0.259i \\ 0.0574 + 0.253i0.0569 + 0.260i0.0566 + 0.252i0.0574 + 0.303i0.0819 + 0.635i0.0566 + 0.302i \\ 0.0570 + 0.238i0.0566 + 0.252i0.0563 + 0.259i0.0570 + 0.259i0.0566 + 0.302i0.0814 + 0.635i \end{bmatrix}(\Omega/\text{km})$$

$$Y_{LS2} = Y_{LR1} = Y_{LT} = 10^{-5}\text{x}\begin{bmatrix} 0.2747i - 0.0588i - 0.0211i - 0.0307i - 0.0200i - 0.0107i \\ -0.0588i0.2900i - 0.0517i - 0.0200i - 0.0206i - 0.0153i \\ -0.0211i - 0.0517i0.2911i - 0.0107i - 0.0153i - 0.0187i \\ -0.0307i - 0.0200i - 0.0107i0.2747i - 0.0588i - 0.0211i \\ -0.0200i - 0.0206i - 0.0153i - 0.0588i0.2900i - 0.0517i \\ -0.0107i - 0.0153i - 0.0187i - 0.0211i - 0.0517i0.2911i \end{bmatrix}(S/km)$$

References

[1] Saha MM, Izykowski JJ, Rosolowski E. Fault location on power networks. 1st ed. London, U.K.: Springer; 2010.
[2] Mahamdedi B, Sanaye-Pasand M, Azizi S, Zhu JG. Unsynchronised fault-location technique for three-terminal lines. IET Gener Transm Distrib 2015;9:2099–107.
[3] Davoudi M, Sadeh J, Kamyab E. Transient-based fault location on three-terminal and tapped transmission lines not requiring line parameters. IEEE Trans Power Deliv 2018;33:179–88.
[4] Miñambres J, Zamora I, Mazon A, Zorrozua M, Alvarez-Isasi R. New technique, based on voltages, for fault location on three-terminal transmission lines. Elect Power Syst Res 1996;37:143–51.
[5] Lin YH, Liu CW, Yu CS. A new fault locator for three-terminal transmission lines-using two-terminal synchronized voltage and current phasors. IEEE Trans Power Deliv 2002;17:452–9.
[6] Evrenosoglu CY, Abur A. Travelling wave based fault location for teed circuits. IEEE Trans Power Deliv 2005;20:1115–21.
[7] Izykowski J, Rosolowski E, Saha MM, Fulczyk M, Balcerek P. A fault-location method for application with current differential relays of three-terminal lines. IEEE Trans Power Deliv 2007;22:2099–107.
[8] Ahmadimanesh A, Shahrtash SM. Time-time-transform-based fault location algorithm for three-terminal transmission lines. IET Gener Transm Distrib 2013;7:464–73.
[9] Gaur VK, Bhalja B. A new faulty section identification and fault localization technique for three-terminal transmission line. Int J Elect Power and Energy Syst 2017;93:216–27.
[10] Mirzaei M, Vahidi B, Hosseinian SH. Fault location on a series-compensated three terminal transmission line using deep neural networks. IET Sci Measur Techno 2018;12:746–54.
[11] Lina T, Xua Z, Ouedraogoa FB, Lee Y. A new fault location technique for three-terminal transmission grids using unsynchronized sampling. Int J Elect Power Energy Syst 2020;123:106229.
[12] Saffarian A, Abasi M. Fault location in series capacitor compensated three-terminal transmission lines based on the analysis of voltage and current phasor equations and asynchronous data transfer. Elect Power Syst Res 2020;187:106457.
[13] Gaur VK, Bhalja BR, Kezunovic M. Novel fault distance estimation method for three-terminal transmission line. IEEE Trans Power Deliv 2020. https://doi.org/10.1109/TPWRD.2020.2984255.
[14] Elsadd MA, Abdelaziz AY. Unsynchronized fault-location technique for two- and three-terminal transmission lines. Elect Power Syst Res 2018;158:228–39.
[15] Cao P, Shu BH, Yang B, et al. Asynchronous fault location scheme based on voltage distribution for three-terminal transmission lines. IEEE Trans Power Deliv 2020;35:2530–40.
[16] Rathore B, Shaik AG. Wavelet-alienation based protection scheme for multi-terminal transmission line. Elect Power Syst Res 2018;161:8–16.
[17] Hussain S, Osman AH. Fault location scheme for multi-terminal transmission lines using unsynchronized measurements. Int J Elect Power and Energy Syst 2016;78:277–84.
[18] Da Silva M, Coury D, Oleskovicz M, Segatto EC. Combined solution for fault location in three-terminal lines based on wavelet transforms. IET Gener Transm Distrib 2010;4:94–103.
[19] Saber A, Emam A, Elghazaly H. New fault location scheme for three-terminal untransposed parallel transmission lines. Elect Power Syst Res J 2018;154:266–75.
[20] Gaur VK, Bhalja B. New fault detection and localisation technique for double-circuit three-terminal transmission line. IET Gener Transm Distrib 2018;12:1687–96.
[21] Ghorbani A, Mehrjerdi EH. Negative-sequence network based fault location scheme for double-circuit multi-terminal transmission lines. IEEE Trans Power Deliv 2019;34:1109–17.
[22] Nagasawa T, Abe M, Otsuzuki N, et al. Development of a new fault location algorithm for multi-terminal two parallel transmission lines. IEEE Trans Power Deliv 1992;7:1516–32.
[23] Funabashi T, Otoguro H, Mizuma Y, Dube L, Ametani A. Digital fault location for parallel double-circuit multi-terminal transmission lines. IEEE Trans Power Deliv 2000;15:531–7.
[24] Sadeh J, Afradi H. A new and accurate fault location algorithm for combined transmission lines using adaptive network-based fuzzy inference system. Elect Power Syst Res J 2009;79:1538–45.
[25] Gilany M, Ibrahim DK, Eldin EST. Traveling-wave-based fault-location scheme for multiend-aged underground cable system. IEEE Trans Power Deliv 2007;22:82–9.
[26] Han J, Crossley PA. Fault location on a mixed overhead and underground transmission feeder using a multiple-zone quadrilateral impedance relay and a double-ended travelling wave fault locator. In: 12th IET International Conference on Developments in Power System Protection (DPSP), Copenhagen, Denmark; 2014:1–6.
[27] Han J, Crossley PA. Fault location on mixed overhead line and cable transmission networks. In: IEEE Grenoble Conference, Grenoble, France; 2013:1–6.
[28] Livani H, Evrenosoglu CY. A machine learning and wavelet-based fault location method for hybrid transmission lines. IEEE Trans Smart Grid 2014;5:51–9.

[29] Gilany M, Eldin EST, Aziz MMA, Ibrahim DK. An accurate scheme for fault location in combined overhead line with underground power cable. In: Proc. IEEE Power Eng. Soc. Gen. Meet., San Francisco, CA, Jun. 12–16, Vol. 3; 2005:2521–27.
[30] Yang X, Choi MS, Lee SJ, Ten CW, Lim SI. Fault location for underground power cable using distributed parameter approach. IEEE Trans Power Syst 2008;23:1809–16.
[31] Liu CW, Lin TC, Yu CS, Yang JZ. A fault location technique for two-terminal multisection compound transmission lines using synchronized phasor measurements. IEEE Trans Smart Grid 2012;3:113–21.
[32] Saber A, Emam A, Elghazaly H. A backup protection approach for multisection compound transmission lines. In: Proc. Eighteenth International Middle East Power Systems Conference (MEPCON), Cairo, Egypt; 2017:1–6.
[33] Zhang S, Gao H, Song Y. A new fault-location algorithm for extra-high-voltage mixed lines based on phase characteristics of the hyperbolic tangent function. IEEE Trans Power Deliv ;31:1203–12.
[34] Lin TC, Lin PY, Liu CW. An algorithm for locating faults in three-terminal multisection nonhomogeneous transmission lines using synchrophasor measurements. IEEE Trans Smart Grid 2014;22:82–9.
[35] Saber A, Emam A, Elghazaly H. A backup protection technique for three-terminal multisection compound transmission lines. IEEE Trans Smart Grid 2018;9:5653–63.
[36] Wu T, Chung CY, Kamwa I, Li J, Qin M. Synchrophasor measurement-based fault location technique for multi-terminal non-homogeneous transmission lines. IET Gener Transm Distrib 2016;10:1815–24.
[37] Lee YJ, Lin TC, Liu CW. Multi-terminal nonhomogeneous transmission line fault location utilizing synchronized data. IEEE Trans Power Deliv 2019;34:1030–8.
[38] Saber A. A new fault location algorithm for multi-terminal mixed lines with shared tower and different voltage levels. IET Gener Transm Distrib 2018;12:2029–37.
[39] Grainger JJ, Stevenson WD. Power system analysis. New York, NY, USA: McGraw-Hill; 1994.
[40] IEEE C37.118.1-2011. IEEE Standard for Synchrophasor Measurements for Power Systems; 2011.